UNIVERSITY OF TARTU

FACULTY OF SCIENCE AND TECHNOLOGY

INSTITUTE OF MOLECULAR AND CELL BIOLOGY

FACULTY OF MEDICINE

INSTITUTE OF BIOMEDICINE AND TRANSLATIONAL MEDICINE

LABORATORY OF PRECISION AND NANOMEDICINE

Assessment of lipid nanoparticle-mediated Cre mRNA delivery in cancer cell lines

Bachelor's thesis

12 EAP

Berit Hiie

Supervisors

Ph.D. Vladimirs Piļipenko

Prof. Tambet Teesalu

Prof. Juhan Sedman

TARTU 2026

Abstracts

Lipiidsete nanoosakeste vahendatud Cre mRNA kohaletoimetamise efektiivsuse hindamine erinevates vähirakkude liinides

Lipiidsed nanoosakesed (LNP-d) on paljulubavad mitteviiruslikud mRNA ja plasmiidse DNA (pDNA) rakusiseseks kohaletoimetamiseks. Rakku penetreerivad peptiidid (CPP-d) ja koesse tungivate peptiididega (TPP-dega) funktsionaliseeritud LNP-d võivad parandada nukleiinhapete rakulist omastamist ja rakusisest transporti. Käesoleva bakalaureusetöö eesmärk oli hinnata CPP-põhiste transfektsioonisüsteemide ja TPP-funktsionaliseeritud LNP-de võimet vahendada funktsionaalset geeniedastust erinevates vähirakkude liinides. Töös kasutati kahekordset Cre reportersüsteemi sisaldavat pDNA konstrukti. Transfekteeritud rakud ekspresseerisid punast fluorestseeruvat valku (RFP), kuid Cre-vahendatud loxP-ga ümbritsetud RFP-STOP kasseti eemaldamine põhjustas fluorestsentsi muutuse RFP-st roheliseks fluorestseeruvaks valguks (GFP). VP1 ja VP4 CPP-sid hinnati pDNA kohaletoimetamise transfektsioonireagentidena, samal ajal kui longCP- ja RPAR-funktsionaliseeritud LNP-sid kasutati Cre mRNA rakusiseseks kohaletoimetamiseks. pDNA ja Cre mRNA kohaletoimetamist ning reportersüsteemi aktivatsiooni hinnati fluorestsentsmikroskoopia ja läbivoolutsütomeetria abil. Kõige tugevamat ja püsivamat Cre reportersignaali täheldati longCP-funktsionaliseeritud LNP-de kasutamisel pärast VP4-vahendatud pDNA transfektsiooni. Käesolev töö näitab CPP-de ja TPP-funktsionaliseeritud LNP-de potentsiaali LNP-vahendatud kohaletoimetamissüsteemide in vitro hindamisel enne nende kasutamist in vivo katsetes.

Märksõnad: lipiidsed nanoosakesed, rakku penetreerivad peptiidid, mRNA kohaletoimetamine, koesse tungivad peptiidid

CERCS kood: B240 Geenitehnoloogia; B260 Molekulaarmeditsiin

Assessment of lipid nanoparticle-mediated Cre mRNA delivery in cancer cell lines

Lipid nanoparticles (LNPs) are promising non-viral delivery systems used for intracellular delivery of mRNA and plasmid DNA (pDNA). Cell-penetrating peptides (CPPs) and tissue-penetrating peptide (TPP)-functionalised LNPs can improve cellular uptake and intracellular transport of nucleic acids. The aim of this bachelor's thesis was to evaluate the ability of CPP-based transfection systems and TPP-functionalised LNPs to mediate functional delivery of pDNA in multiple cancer cell lines. A dual Cre reporter pDNA construct was used in this study. Transfected cells expressed red fluorescent protein (RFP), while Cre-mediated excision of the loxP-flanked RFP-STOP cassette resulted in a fluorescence switch from RFP to green fluorescent protein (GFP). VP1 and VP4 CPPs were evaluated as transfection reagents for pDNA delivery, whereas longCP- and RPAR-functionalised LNPs were used for intracellular delivery of Cre mRNA. Delivery efficiency and reporter activation were analysed using fluorescence microscopy and flow cytometry. The strongest and most sustained Cre reporter activation was observed in cells treated with longCP-functionalised LNPs following VP4-mediated pDNA transfection. These results demonstrate the potential of CPPs and TPP-functionalised LNPs for in vitro evaluation of LNP-mediated delivery systems prior to in vivo applications.

Keywords: lipid nanoparticles, cell-penetrating peptides, mRNA delivery, tissue-penetrating peptides

CERCS code: B240 Gene technology; B260 Molecular medicine

Table of Contents

Abbreviations

ApoE	Apolipoprotein E
CPP	Cell-penetrating peptide
DMEM	Dulbecco's Modified Eagle's Medium
DPBS	Dulbecco’s Phosphate-Buffered Saline
DSPC	1,2-distearoyl-sn-glycero-3-phosphocholine
FBS	Fetal bovine serum
GFP	Green fluorescent protein
LNPs	Lipid nanoparticles
LongCP	Long cerepep
MEM	Minimal Essential Medium
MQ	Milli-Q water
NRP1	Neuropilin 1
Opti-MEM	Optimized Minimal Essential Medium
pDNA	Plasmid DNA
RFP	Red fluorescent protein
scrLongCP	Scrambled long cerepep
siRNA	small interfering ribonucleic acid
TBST	Tris-Buffered Saline containing Tween-20
TPP	Tissue-penetrating peptide

Introduction

Lipid nanoparticles (LNPs) have emerged as one of the most promising non-viral delivery platforms for transporting different types of nucleic acids, including messenger mRNA, small interfering ribonucleic acids (siRNA) and plasmid DNA (pDNA) into cells (Hou et al., 2021). Compared to viral vectors, LNPs offer several advantages, such as lower immunogenicity, improved safety profile and easier large-scale production (Cullis & Hope, 2017). However, efficient intracellular delivery remains challenging, since nucleic acid cargo must avoid endosomal degradation after cellular uptake and successfully reach the cytoplasm or nucleus in a biologically active form (Sahay et al., 2013). Therefore, considerable effort has been directed towards developing strategies that improve nanoparticle uptake and intracellular transport.

One possible approach is the use of cell-penetrating peptides (CPPs) and tissue-penetrating peptides (TPPs). CPPs are able to form complexes with nucleic acids and facilitate their cellular uptake through electrostatic interactions with the cell membrane (Guidotti et al., 2017). In addition, TPPs, including longCP- and RPAR-based systems, may improve nanoparticle binding to target cells and enhance intracellular transport and tissue penetration (Sugahara et al., 2009; Teesalu et al., 2012). Such peptide-functionalised delivery systems may improve delivery efficiency while reducing non-specific accumulation outside the target tissue.

Reporter systems are commonly used to evaluate gene delivery efficiency because they allow assessment not only of nanoparticle uptake, but also of functional intracellular delivery. In this study, the Cre/Ai9 reporter system was used, where tdTomato fluorescence is activated only after Cre recombinase removes LoxP-flanked STOP cassette (Madisen et al., 2012). This system therefore enables evaluation of whether the delivered nucleic acid cargo retains biological activity after intracellular delivery.

The aim of this bachelor's thesis was to evaluate the efficiency of non-viral delivery using CPP-mediated transfection systems and peptide-functionalised LNPs in different cancer cell lines. The work was carried out at the Laboratory of Precision and Nanomedicine at the Institute of Biomedicine and Translational Medicine, Faculty of Medicine, University of Tartu.

1. Literature Review

1.1 Lipid Nanoparticles

Lipid nanoparticles are non-viral vectors used to deliver nucleic acids such as siRNA, mRNA and DNA and are characterized by their versatility, biocompatibility, biodegradability and effectiveness in vivo (Vasudevan et al., 2025). LNPs have become a key delivery platform for nucleic acid-based therapies due to their ability to protect genetic material, enhance cellular uptake and enable endosomal escape (Alshehry et al., 2025). As a result, they are used in applications ranging from delivery of mRNA drugs and personalized cancer vaccines to systemic gene editing strategies (Alshehry et al., 2025).

The effectiveness of LNPs in different applications is largely determined by their physicochemical properties and composition (Alshehry et al., 2025). LNPs generally consist of four components: ionizable lipid, phospholipid, cholesterol and polyethylene glycol (PEG)ylated lipid, each contributing to particle stability, transfection efficiency and safety (Zong et al., 2023; Figure 1). Parameters such as particle size, surface charge and lipid composition determine the ability of LNPs to protect nucleic acids from degradation and facilitate their delivery into target cells (Alshehry et al., 2025). Experimental studies have shown that LNP morphology and internal organisation are strongly affected by the lipid composition and the type of nucleic acid cargo, meaning that LNPs should not be considered as uniform carrier particles but as structurally complex formulations (Eygeris et al., 2020; Kulkarni et al., 2018).

Several studies have further shown that selective cellular targeting is a key determinant of therapeutic efficacy, duration of action and overall safety (Cullis & Hope, 2017; Hou et al., 2021). For example, optimizing the ratio of ionizable lipids to cholesterol can enhance particle stability, improve mRNA translation efficiency and strengthen immune responses, which is particularly important in cancer therapy (Eygeris et al., 2022; Kulkarni et al., 2018). Moreover, surface functionalization with targeting ligands, such as antibodies or peptides, enables tumour-specific delivery, thereby reducing off-target exposure and minimizing toxicity in healthy tissues (Tang et al., 2023). Figure 1 highlights how the different lipid components are spatially organised within the nanoparticle and contribute to its delivery function.

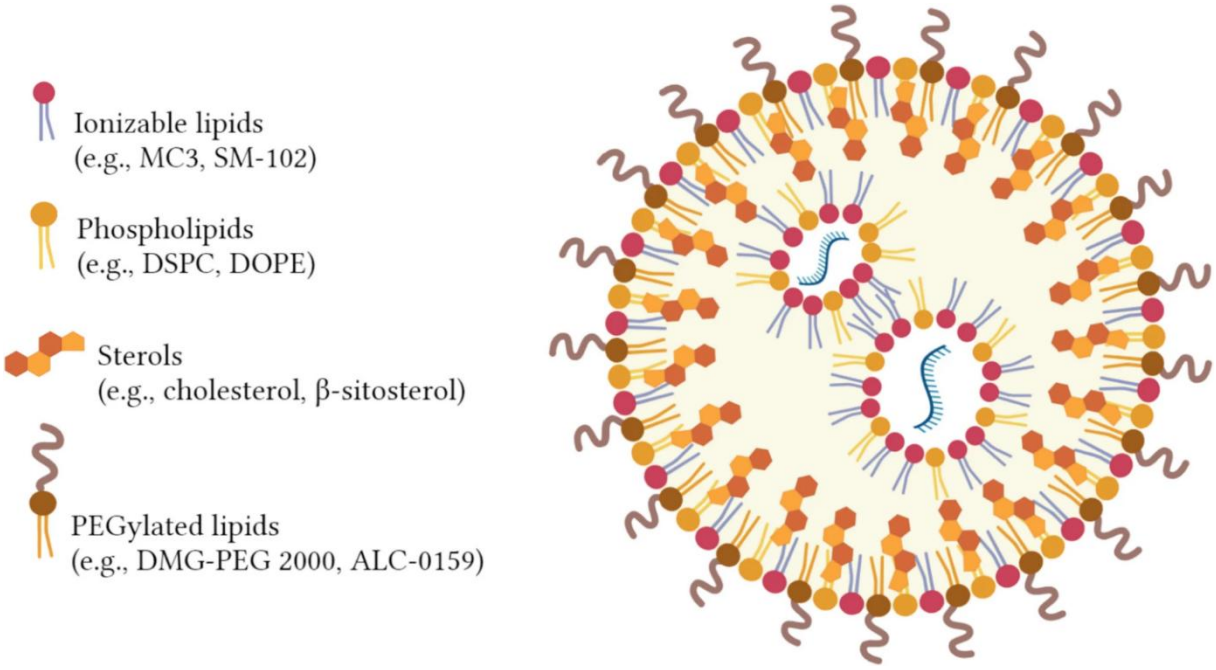

Figure 1. Schematic representation of lipid nanoparticle structure and composition, showing ionizable lipids, phospholipids, cholesterol and PEGylated lipids surrounding an mRNA core. DMG, dimyristoyl glycerol; DOPE, Dioleoyl phosphatidylethanolamine; DSPC, 1,2-distearoyl-sn-glycero-3-phosphocholine. Illustration from Alshehry et al., 2025.

Each component of LNPs serves a specific function that collectively enable efficient nucleic acid delivery (Zong et al., 2023). Ionizable lipids act as pH responsive switches that enable high-efficiency nucleic acid loading under acidic conditions, render LNPs stealthy in the bloodstream and trigger membrane disruptive non bilayer phases within the acidic endosome to achieve cytosolic release (Cullis & Hope, 2017). The importance of ionizable lipid structure is also supported by studies showing that changes in lipid chemistry can markedly affect LNP potency, tolerability and endosomal escape efficiency (Eygeris et al., 2022; Tang et al., 2023). Phospholipids such as 1,2-distearoyl-sn-glycero-3-phosphocholine (DSPC) provide a structural bilayer that stabilizes LNPs, regulates their size and morphology, supports efficient nucleic acid encapsulation and acts as a charge-diluting scaffold that facilitates optimal surface charge and promotes lipid mixing during endosomal escape (Cullis & Hope, 2017; Kulkarni et al., 2019). Cholesterol plays a critical role in LNP structure and function by stabilizing the particle surface, modulating membrane rigidity and curvature and influencing particle size and morphology, while also supporting the formation of lipid-nucleic acid complexes that enhance encapsulation efficiency and overall mRNA or siRNA delivery performance (Eygeris et al., 2020; Kulkarni et al., 2019). Helper lipids are not only structural components but can influence the organisation, stability and delivery activity of LNPs, which is why apparently small changes in lipid composition can lead to different biological outcomes (Kulkarni et al., 2019). PEGylated lipids are incorporated into LNPs to form a hydrated surface layer that prevents aggregation and maintains a narrow size distribution, thereby enhancing colloidal stability (Hou et al., 2021).

Located in the outer leaflet, PEG lipids create a stealth effect that reduces protein adsorption and opsonisation, limiting clearance by the mononuclear phagocyte system and prolonging circulation time (Eygeris et al., 2022; Hou et al., 2021). Their proportion and molecular weight also influence particle size, surface charge and delivery efficiency, while functionalisation of PEG termini enable targeted delivery (Cullis & Hope, 2017; Hou et al., 2021). Importantly, PEG acts as a transient steric shield that stabilizes LNPs during circulation but can dissociate to allow efficient cellular uptake and endosomal escape (Cullis & Hope, 2017).

The internal structure of LNPs is more complex than a simple amorphous core, as both the RNA cargo and lipid composition contribute to the formation of distinct structural architectures (Eygeris et al., 2020). These can include homogeneous cores, bilamellar particles (two lipid layers), multilamellar "onion like" structures (multiple concentric layers) and polymorphic particles with internal defects (Eygeris et al., 2020). In certain formulations, mRNA has been shown to influence lipid organisation by promoting bilayer-like arrangements of ionisable lipids and reducing the presence of amorphous solid cores, indicating that RNA plays active role in shaping nanoparticle structure rather than being passively encapsulated (Eygeris et al., 2020; Kulkarni et al., 2019). In addition, helper lipids and sterols modulate membrane organisation and determine whether particles remain structurally uniform or develop multilamellar and phase-separated domains (Eygeris et al., 2020). These structural variations are not merely descriptive but have functional consequences, as particles with more complex or multilamellar architectures have been associated with improved transfection efficiency (Eygeris et al., 2020).

1.1.1. LNP Mediated Delivery Systems

Building on the structural components described above, the effectiveness of LNPs depends on their ability to deliver nucleic acids into target cells and release them into the cytosol. Following cellular uptake, LNPs are primarily internalised through macropinocytosis, a process that depends on endosomal acidification (Sahay et al., 2013). After internalisation, LNPs are trafficked to late endosomes and lysosomes, where a large proportion of the nucleic acid cargo is either degraded or recycled back out of the cell, limiting delivery efficiency (Sahay et al., 2013). As a result, intracellular trafficking and endosomal escape represent major barriers, since only a small fraction of the cargo successfully reaches the cytosol (Sahay et al., 2013). This limitation is important because successful cellular uptake does not necessarily mean successful functional delivery; LNPs may enter cells but still fail to release sufficient cargo into the cytosol for detectable gene expression changes (Sahay et al., 2013).

The efficiency of delivery is further influenced by nanoparticle composition, as lipid properties affect intracellular processing and release (Eygeris et al., 2020; Hou et al., 2021). For this reason, recent research has focused on optimising LNP design for improved organ- and cell-specific delivery. Strategies such as modifying lipid composition have been shown to redirect expression beyond the liver to tissues such as the spleen or lung, while local delivery approaches enable gene expression in sites such as the eye (Cheng et al., 2020; Vasudevan et al., 2025). For example, selective organ targeting nanoparticles demonstrated that modifying the lipid composition can shift mRNA delivery and protein expression toward specific tissues, supporting the idea that LNP biodistribution can be engineered rather than fixed (Cheng et al., 2020). However, achieving precise targeting and efficient cytosolic delivery remains a significant challenge due to both biological and physicochemical limitations (Xu & Xia, 2023), as LNPs preferentially accumulate in the liver through apolipoprotein E (ApoE)-medited uptake, while inefficient endosomal escape limits the amount of nucleic acid that can reach the cytosol and drive gene expression (Hou et al., 2021).

Following successful cytosolic delivery, mRNA must be sufficiently stable and efficiently translated to produce functional protein. However, intracellular degradation and immune recognition can limit this process (Hou et al., 2021). Exogenous mRNA is susceptible to degradation by cellular nucleases, which reduces its availability for translation (Hou et al., 2021; Xu & Xia, 2023). In addition, innate immune sensing pathways can recognise foreign RNA and trigger responses that suppress protein synthesis, further decreasing expression efficiency (Alshehry et al., 2025; Hou et al., 2021). Structural features and chemical modifications of mRNA, including nucleoside modification and removal of double stranded RNA contaminants, help reduce immune activation and improve translation efficiency (Hou et al., 2021).

Once expressed, mRNA driven protein production is usually transient rather than permanent, allowing controlled, time limited expression without genomic integration (Hou et al., 2021). The magnitude and duration of expression can vary depending on tissue type and nanoparticle formulation (Cheng et al., 2020). For example, intracameral LNP delivery in the eye produced strong reporter expression that peaked around 72 hours and declined by approximately 120 hours, indicating a defined but limited expression window (Vasudevan et al., 2025). In contrast, selective organ-targeting LNPs can modify biodistribution and redirect expression to tissues such as the spleen or lung, with some formulations maintaining detectable protein expression for more than one week (Cheng et al., 2020). These findings demonstrate that both nanoparticle design and tissue context play a key role in determining the magnitude and duration of mRNA

expression following delivery. This is particularly relevant in reporter systems such as Ai9, where sufficient protein expression is required to generate a detectable fluorescent signal.

1.1.2. Limitations of Lipid Nanoparticles

Despite their success in enabling clinical mRNA delivery, LNPs present several important limitations related to safety, targeting and delivery efficiency, particularly in the context of cancer immunotherapy (Alshehry et al., 2025). Clinical responses to LNP-based mRNA vaccines remain variable, with only a subset of patients achieving durable tumour regression (Alshehry et al., 2025). A major limitation is inefficient endosomal escape, as only a small proportion of internalised nanoparticles successfully release their mRNA cargo into the cytosol, thereby limiting protein expression and antigen presentation (Alshehry et al., 2025; Eygeris et al., 2020; Hou et al., 2021). This has been shown experimentally for LNP-mediated siRNA delivery, where endocytic recycling was identified as a major reason why internalised cargo does not efficiently reach the cytosol (Sahay et al., 2013). In addition, LNPs exhibit biased biodistribution, accumulating predominantly in the liver and spleen due to ApoE-mediated uptake, which restricts delivery to extra-hepatic tumours and necessitates extensive optimisation of lipid composition (Alshehry et al., 2025; Hou et al., 2021; Xu & Xia, 2023). Therefore, newer LNP design strategies increasingly focus on modifying lipid composition or surface properties to improve extrahepatic delivery and reduce unwanted accumulation in non-target tissues (Cheng et al., 2020; Xu & Xia, 2023). LNP performance is also highly sensitive to formulation, as small changes in lipid ratios or sterol structure can significantly alter particle morphology, stability and gene expression, reflecting a complex and still poorly predictable structure-activity relationship (Eygeris et al., 2020; Xu & Xia, 2023). Safety and immunological concerns further complicate their use, as ionizable lipids and mRNA can trigger innate immune responses and inflammatory toxicity, while PEGylated lipids may induce hypersensitivity reactions and anti-PEG antibodies upon repeated dosing (Alshehry et al., 2025; Hou et al., 2021; Xu & Xia, 2023). Additional challenges include limited tumour-specific targeting, difficulty crossing biological barriers such as the blood-brain barrier, transient protein expression requiring repeated administration and the need for biodegradable lipid chemistries to reduce accumulation-related toxicity (Alshehry et al., 2025; Xu & Xia, 2023). Furthermore, LNP formulations require strict storage conditions and involve complex, costly manufacturing processes, which complicate large-scale and personalised therapeutic applications (Alshehry et al., 2025; Hou et al., 2021). Collectively, these limitations highlight the need for continued optimisation of LNP design to improve safety, targeting precision and therapeutic efficacy.

1.1.3. Barriers to Nanoparticle Delivery in Cancer

Cancer drug delivery is challenging because the tumour microenvironment is a complex and abnormal system rather than a passive target (Jain, 2013). It consists of malignant cells, stromal cells, vascular networks and extracellular matrix components that together create multiple barriers to effective therapy (Jain, 2013). Blood flow within tumours is often irregular and heterogeneous, leading to poorly perfused regions that limit the access of circulating therapeutics and immune cells, while also contributing to conditions such as low pH and hypoxia (Jain, 2013). Hypoxia further promotes tumour progression and reduces the effectiveness of therapies that rely on oxygen availability or proper vascular function (Jain, 2013). In addition, the dense extracellular matrix acts as both a physical and biochemical barrier, restricting the penetration of therapeutic agents, while stromal remodelling and collagen rich structures can further hinder their distribution within tumour tissue (Blanco et al., 2015; Jain, 2013). Together, these factors result in uneven drug distribution, limited tumour penetration and increased resistance to treatment and disease progression (Jain, 2013). For nanoparticle-based delivery systems, presence of tumour associated barriers means that successful systemic circulation is not sufficient; particles must also extravasate, penetrate tumour tissue, enter target cells and release their cargo intracellularly (Blanco et al., 2015; Jain, 2013). These barriers are particularly relevant for nanoparticle-based delivery systems, as they limit tumour penetration, cellular uptake and overall therapeutic efficiency.

1.2. Delivery of payloads with peptides

1.2.1. Cell-penetrating peptides

CPPs are short peptides that can cross cellular membranes through both energy-dependent and energy-independent mechanisms and are widely used as delivery vectors for biologically active cargoes (Guidotti et al., 2017). They are particularly useful because many therapeutic molecules, including proteins, peptides and nucleic acids, are too large or too hydrophilic to efficiently enter cells on their own (Bechara & Sagan, 2013; Guidotti et al., 2017). However, CPP-mediated delivery is also limited by variable uptake mechanisms, possible endosomal entrapment and differences in efficiency depending on the cargo, peptide sequence and cell type (Bechara & Sagan, 2013; Erazo-Oliveras et al., 2014; Guidotti et al., 2017). For pDNA delivery, CPPs typically form non-covalent complexes with nucleic acids through electrostatic interactions between positively charged peptides and negatively charged DNA, which can enhance cellular uptake and provide some protection from degradation (Guidotti et al., 2017).

Cellular internalisation can occur via direct membrane translocation or endocytosis, although these mechanisms may operate simultaneously depending on the peptide, cargo and experimental conditions (Bechara & Sagan, 2013). Following endocytosis uptake, efficient endosomal escape is required for functional delivery, as entrapment within endosomes significantly limits intracellular activity (Erazo-Oliveras et al., 2014). As a result, CPPs are widely used as non-viral delivery strategy to improve intracellular transport, although overcoming endosomal escape remains a major challenge (Erazo-Oliveras et al., 2014; Guidotti et al., 2017).

In this study, two CPP formulations produced by Vectiopep (Estonia) – VP1 and VP4 – were investigated as pDNA delivery systems. Vectiopep CPP technology has been developed to improve selective intracellular transport of mRNA into immune related tissues and cells, particularly antigen presenting cells, with the aim of enhancing cancer immunotherapy approaches (Vectiopep, n.d.). Unlike conventional LNP systems, which often accumulate predominantly in the liver, CPP-based delivery systems have been designed to promote more selective extrahepatic delivery, including targeting towards lymphoid tissues such as the spleen (Porosk et al., 2023). Because CPP-mediated delivery efficiency depends strongly on intracellular trafficking and endosomal escape, evaluating the transfection efficiency of different CPP formulations was an important objective of this work (Erazo-Oliveras et al., 2014; Guidotti et al., 2017).

1.2.2. Tissue-penetrating Peptides

TPPs are a distinct group of peptides that can improve delivery not only into cells, but also deeper into the target tissue, which helps address the limited tissue distribution seen with many conventional targeting strategies (Sugahara et al., 2009). One of the best-known examples is iRGD, which first binds to α_v integrins and is then proteolytically cleaved to expose a C-terminal CendR motif that binds the neuropilin-1 (NRP1) receptor, promoting further transport into cells and surrounding tissues (Sugahara et al., 2009; Teesalu et al., 2012). This multistep process promotes deeper transport into tumour tissue and enhances the intratumoral distribution of therapeutic agents (Sugahara et al., 2009, 2010). For this reason, TPPs have attracted considerable interest as targeting ligands for nanoparticles and other delivery systems in cancer therapy, where inefficient penetration into poorly accessible tumour regions remains a major obstacle (Blanco et al., 2015; Sugahara et al., 2010). Because several TPPs function through NRP1-mediated transport pathways, they are also relevant for nanoparticle targeting strategies investigated in this work.

1.3. Reporter systems for quantifying nucleic acid delivery

Reporter systems are widely used in biological research because they convert otherwise difficult to observe biological events into measurable signals (Madisen et al., 2010; Vasudevan et al., 2025). This enables researchers to monitor gene expression, recombination and delivery outcomes in a clear quantifiable manner (Cheng et al., 2020; Madisen et al., 2010). Reporter systems are used because mRNA delivery is not directly observable and a measurable readout is required to determine whether the cargo has reached the target tissue, been translated and produced a functional signal (Cheng et al., 2020; Vasudevan et al., 2025). In LNP studies, reporters such as luciferase, tdTomato and mCherry enable quantification of delivery efficiency, comparison of different formulations and evaluation of the duration of expression in specific tissues or cell types (Cheng et al., 2020). Importantly, reporter systems distinguish between successful localisation of the nanoparticle and successful intracellular expression, which is essential when assessing whether a given LNP formulation is functionally effective in vivo (Vasudevan et al., 2025). This distinction is essential in LNP studies because delivery efficiency can be overestimated if only nanoparticle uptake is measured, while reporter activation confirms that the delivered cargo produced a biological effect inside the cell (Cheng et al., 2020; Sahay et al., 2013). As a result, reporter expression provides a standardised and practical proxy for transfection efficiency, tissue selectivity and gene-editing performance (Cheng et al., 2020). In the Ai9 system, this is particularly relevant because detectable tdTomato fluorescence depends on sufficient expression of functional Cre recombinase following delivery

1.3.1. Ai9 reporter system

The Ai9 reporter system is a Cre recombinase dependent fluorescent reporter model, in which a loxP-flanked STOP cassette prevents expression of the tdTomato gene (Vasudevan et al., 2025).

Cre recombinase originates from bacteriophage P1, which infects *Escherichia coli*, where it functions as a 38 kDa enzyme that mediates site-specific recombination to resolve concatemeric phage DNA into monomeric circles required for viral packaging (Sauer & Henderson, 1988). The enzyme recognises 34 bp loxP sequences and is unique in that it requires no additional host factors or cofactors to catalyse recombination, making it a highly versatile genetic tool (Sauer & Henderson, 1988). This simplicity enabled its adaption for use in eukaryotic systems, as demonstrated by Sauer and Henderson (1988), who showed that Cre could efficiently mediate precise recombination in mammalian cells, establishing the foundation for its widespread use in genome engineering applications.

Cre recombinase recognises loxP sites through specific interactions with their defined 34 bp DNA structure, which consists of 13 bp inverted repeats flanking an 8 bp spacer region (Hoess et al., 1982). The inverted repeats function as binding sites for Cre, while the central spacer determines the position of strand cleavage (Hoess et al., 1982). Binding of Cre to each repeat results in the formation of dimeric complex and when two loxP sites are present, these complexes assemble into tetrameric synaptic structure that aligns the DNA for recombination (Hoess et al., 1982; Sauer & Henderson, 1988). Efficient recombination depends on the integrity and symmetry of the inverted repeats, as sequence alterations in these regions reduce Cre activity (Hoess et al., 1982). This precise arrangement of binding and catalytic elements ensures accurate and site-specific recombination (Hoess et al., 1982).

The Ai9 mouse, developed by Allen Institute as part of Rosa26-trageted "Ai" reporter series, contains a strong CAG promoter and WPRE enhancer controlling tdTomato expression (Madisen et al., 2010). tdTomato is a red fluorescent protein derived from *Discosoma sp.* engineered as a tandem dimer to provide exceptionally high brightness and photostability compared to earlier red fluorophores (Shaner et al., 2004). tdTomato absorbs light at 554 nm and emits red light at 581 nm (Shaner et al., 2004). It is among the brightest fluorescent proteins reported, allowing direct detection of reporter expression by fluorescence microscopy or flow cytometry without antibody amplification (Madisen et al., 2010; Shaner et al., 2004). When Cre recombinase is present, it removes the STOP cassette, allowing tdTomato to be permanently expressed and producing a strong fluorescent signal specifically in Cre-positive cells, with minimal background expression in cells lacking Cre (Madisen et al., 2012). Because tdTomato expression is activated only after functional Cre recombinase reaches the cell and mediates recombination, the Ai9 system provides a functional readout of successful intracellular delivery rather than only measuring particle uptake or localisation (Cheng et al., 2020; Madisen et al., 2010). When there is no Cre recombinase present, the STOP cassette prevents signal activation and there in no fluorescent signal (Madisen et al., 2012). This process is illustrated schematically in Figure 2.

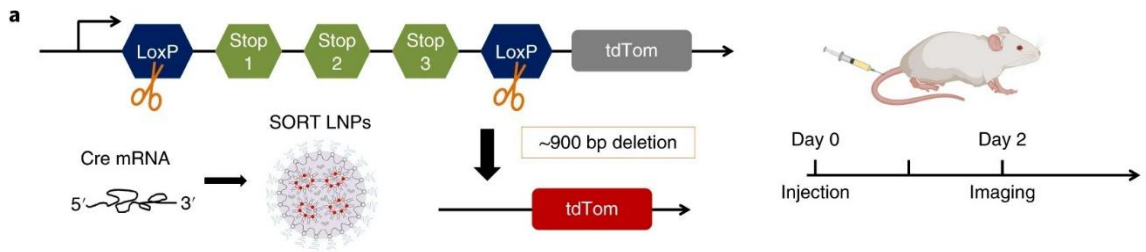

Figure 2. Schematic representation of Ai9 reporter activation following LNP-mediated Cre mRNA delivery. SORT, selective organ targeting; tdTom, TdTomato. Adapted from Cheng et al., 2020.

The Ai9 reporter system is experimentally useful because it provides a bright and sensitive readout of Cre activity, with tdTomato expression that is substantially stronger than earlier Rosa26-based reporters such as EYFP, making it easier to detect using fluorescence imaging, histology and flow cytometry (Madisen et al., 2010). In addition, the system is well suited for lineage tracing as the reporter remains inactive until Cre-mediated recombination removes loxP-flanked STOP cassette, resulting in stable labelling of recombined cells (Cheng et al., 2020; Madisen et al., 2010). This enables long term tracking of cell fate in vivo. Together, the combination of high signal intensity, low background in unrecombined cells and irreversible activation makes the Ai9 system a robust tool for validating delivery, tracking recombination events and quantifying gene editing efficiency (Cheng et al., 2020; Madisen et al., 2010).

2. Experimental part

2.1 Aims of the study

The aim of this study was to evaluate and compare non-viral gene delivery strategies, including CPP-based cell transfection and LNP-mediated Cre mRNA delivery, using in vitro and in vivo reporter systems to assess the efficiency of functional delivery. The objectives of the study were to:

1. Perform multiple cell line transfection with CPPs and determine the optimal transfection conditions;
2. Demonstrate that decorating LNPs with TPPs improves their binding and cellular entry;
3. Assess whether these delivery approaches enable functional reporter activation both in vitro and in vivo.

2.2 Materials and Methods

In this study, multiple human and murine cell lines were used as models for evaluating transfection and delivery efficiency. The characteristics and sources of the cell lines are summarized in Table 1.

Table 1. Characteristics and sources of cell lines used in this study.

Cell line	Description	Source
DU145	Human prostate carcinoma cell line (Stone et al., 1978)	ATCC, HTB-81 (United States of America)
M21	Human melanoma cell line (Brooks et al., 1994)	Acquired from Erkki Ruoslahti's research group, Sanford Burnham Preby Medical Discovery Institute, California
PPC1	Human prostate adenocarcinoma cell line (Brothman et al., 1989)	Acquired from Erkki Ruoslahti's research group, Sanford Burnham Preby Medical Discovery Institute, California

Neuro2a	Mouse neuroblastoma cell line (Olmsted et al., 1970)	ATCC, CCL-131 (United States of America)
GL261	Murine glioma cell line (Szatmári et al., 2006)	Donated by Flavio Curnis from San Raffaele Scientific Institute, Milan, Italy

Cells were cultured in an incubator at 37°C with 5% CO_2 in Dulbecco's Modified Eagle's Medium (DMEM) or Minimum Essential Medium (MEM) supplemented with 10% Fetal bovine serum (FBS) and 1% Pen Strep; 1% non-essential amino acid solution (100X) was also added to MEM. Opti-MEM was used during transfection experiments and Dulbecco's Phosphate-Buffered Saline (DPBS) was used for washing and resuspension of cells. Media and reagents used in this study are summarized in Table 2.

Table 2. Culture media and reagents used in this study.

Media	**Application**	**Source**
Dulbecco's Modified Eagle Medium (DMEM)	Media for M21, PPC1, GL261 cells	Capricorn Scientific, cat. no. DMEM-HPA
Minimum Essential Medium (MEM) with Earle's Salts	Media for Neuro2a and DU145 cells	Capricorn Scientific, cat. no. MEM-A
Non-essential amino acid solution (100x)	Supplement for Neuro2a and DU145 media	Sigma-Aldrich, cat. no. M7145-100ML
Optimized Minimal Essential Medium (Opti-MEM)	Used during transfection (all cell lines)	Thermo Fisher Scientific, cat. no. 31985070
Dulbecco's Phosphate-Buffered Saline (DPBS)	For washing cells, all cell lines	Corning, cat. no. 21-031-CV
CellStripper®	For detaching cell lines, all cells	Corning, cat. no. 25-056-Cl
Fetal bovine serum (FBS)	Supplement for all media	Capricorn Scientific, cat. no. FBS-11A

UltraPure™ DNase/RNase-Free Distilled Water	Diluting pDNA/transfection reagents	ThermoFisher Scientific, cat. no. 10977035

In this study VP1 and VP4 CPPs (generously provided by Piret Arukuusk, Vectiopep, Estonia) were used for peptide-mediated nucleic acid delivery. These peptides are designed to facilitate intracellular uptake through formation of peptide-nucleic acid complexes and enhanced cellular internalisation (Guidotti et al., 2017). In addition, longCP-, RPAR- and scrambled peptide-functionalised LNPs were used to evaluate peptide-mediated targeting and intracellular delivery. Cerepep is an unpublished brain-targeting peptide previously identified in the laboratory of precision and nanomedicine through in vivo phage display screening. RPAR is a NRP1-binding CendR peptide associated with enhanced cellular uptake and tissue penetration (Sugahara et al., 2009; Teesalu et al., 2009).

For transfection experiments, pDNA construct encoding fluorescent reporter system was used, including a dual DsRed/eGFP Cre reporter plasmid (Figure 3). The dual reporter plasmid allows visualisation of Cre-mediated recombination through fluorescence switching from red to green signal.

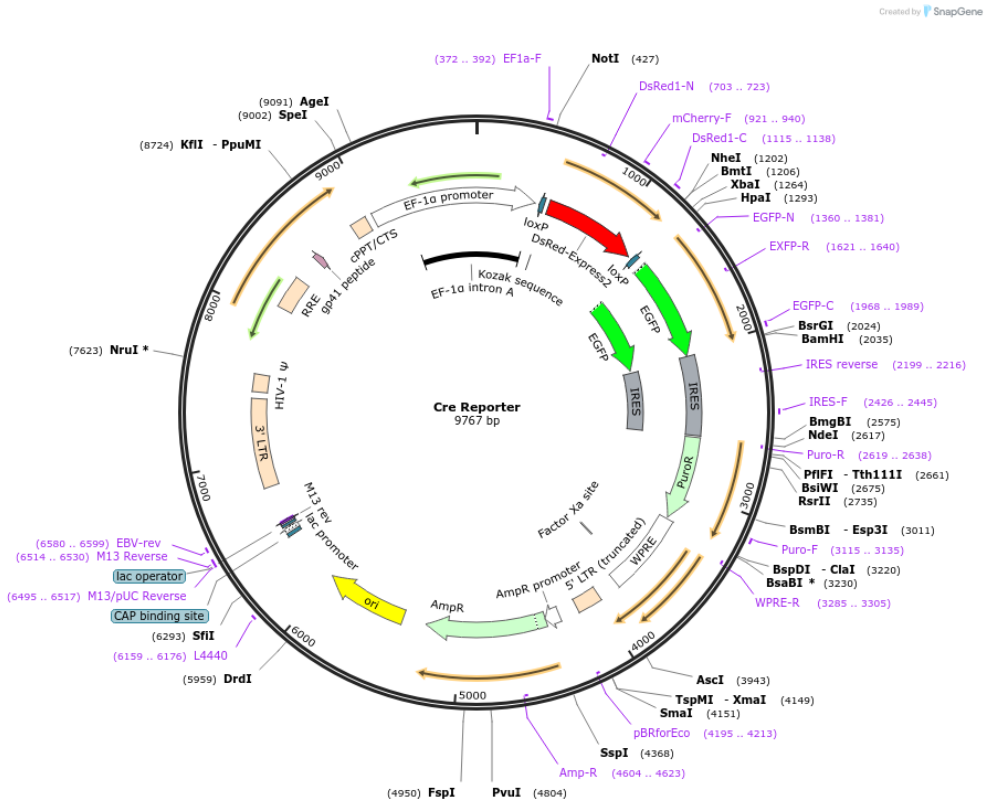

Figure 3. Schematic representation of the dual DsRed/eGFP Cre reporter construct used in transfection experiments. The plasmid contains a loxP-flanked DsRed-Express2 cassette upstream of the EGFP reporter, enabling Cre-mediated switching from red to green

fluorescence following recombination. Illustration form Addgene plasmid repository (plasmid #62732) originally described by (D'Astolfo et al., 2015).

2.2.1 Preparing Cell Lysates for Western Blotting

Cell media was aspirated from confluent cells and cells were washed with PBS. After washing 5-10 ml of media was added to cells. With the scraper tool, cells were detached from the flask and transferred to a 15 ml tube, then centrifuged in Eppendorf 5810 R at 200-300g at 4°C for 5 minutes.

The tubes were returned to a Class I, type A2 biological safety cabinet (Esco Labculture) and media was carefully aspirated. Pellet was resuspended in 1 ml of dPBS, then transferred to 1.5 ml Eppendorf tube and put on ice. Cells were centrifuged in Eppendorf 5424R centrifuge at 200-300g at 4 °C for 7 minutes.

After centrifugation PBS was removed and 50 µl of lysis buffer was added to the cells and mixed with a pipette. Tubes were left on ice for 30 minutes, then centrifuged in Eppendorf 5424R centrifuge at 14000g at 4 °C for 10 minutes.

The supernatant was collected without touching the pellet and transferred to a new tube. Tubes were put at -80 °C until use.

2.2.2 Western Blot

Protein samples were mixed with 4X Laemmli sample buffer and denatured at 95°C for 5 minutes prior to loading onto the BioRad Mini-PROTEAN SDS-PAGE gels. Electrophoresis was performed in 1X Tris-Glycine running buffer at 80-100 V until adequate protein separation was achieved.

Following electrophoresis, proteins were transferred onto a 0.2 µm PVDF membrane using the Trans-Blot Turbo Transfer System with prepackaged Trans-Blot Turbo Mini transfer packs (BioRad, cat. no. 1704156).

The bottom (+) ion reservoir stack containing the membrane was placed onto the cassette base (anode). The gel was carefully positioned on top of the membrane and air bubbles were removed using a blot roller. The top (–) ion reservoir stack was then placed over the gel to complete the transfer sandwich. The cassette was closed, locked and inserted into the instrument bay.

Protein transfer was performed using the preprogrammed Mixed Molecular Weight (Turbo) protocol (25 V, 1.3 A, 7 minutes) for a single mini gel, according to the manufacturer's

recommendations. Upon completion, membranes were immediately removed for downstream processing.

Membranes were blocked for 1 hour at room temperature in blocking buffer – 5% non-fat dry milk in Tris-buffered saline containing 0.1% Tween-20 (TBST) to prevent non-specific binding. Anti-NRP1 primary antibody was diluted in the same blocking buffer at 1:500 concentration and incubated with the membranes with gentle agitation at 4 °C overnight.

Following primary antibody incubation, membranes were washed three times for 5 minutes each in TBST. Membranes were then incubated with appropriate horseradish peroxidase-conjugated goat anti-mouse antibody diluted 1:5000 in blocking buffer for 1 hour at room temperature. After this incubation, membranes were washed three times for 5 minutes each in TBST and photographed using Li-Cor Odyssey® imaging system.

2.2.3 Transfection with VP1 and VP4 peptides

Transfection of pDNA was tested using VP1 and VP4 CPPs (peptide sequences are proprietary). Cells were seeded in 24-well plates one day prior to transfection. PPC1, M21, Neuro2a and GL261 cells were seeded at a density of 4×10^4 cells per well, while DU145 cells were seeded at a density of 9.5×10^4 cells per well to account for differences in growth characteristics.

For transfection, pDNA encoding the dual DsRed/eGFP reporter was used at a final amount of 500 ng per well. Three microlitres of pDNA was diluted in Milli-Q (mQ) water to achieve the required volume for complex formation. Both VP1 and VP4 peptides were diluted to 100 µM concentration, and four different charge ratios (CR 1.5, 2, 2.5 and 3) were tested. The charge ratio refers to the ratio between positively charged peptide and negatively charged pDNA, which influences complex formation and transfection efficiency.

Briefly, pDNA was added to mQ water, followed by addition of the appropriate amount of VP1/VP4, thoroughly mixed and left to incubate for 20 min at room temperature for complex formation. After that, 100 µl of the mixture was added dropwise onto the cells and the plate was swirled to evenly distribute the mixture.

Cells were incubated with the transfection complexes under standard culture conditions (37°C, 5% CO_2). At 24 and 48 hours post-transfection, cells were checked for RFP expression by fluorescence microscopy. After transfection cells were kept in full media for 24 h and then incubated with TPP-decorated Cre mRNA encapsulating LNPs, and nucleic acid delivery was determined by fluorescence microscopy and flow cytometry.

2.2.4 LNP Preparation Using Microfluidic System

First, LNPs were first prepared with polyadenylic acid (polyA) encapsulated. PolyA is a synthetic RNA sequence made entirely of adenosine residues; it is much cheaper than mRNA and can be used to predict encapsulation in LNPs. Lipid stock solutions were prepared in pure ethanol and polyA stocks in 25 mM sodium acetate. Tubing for nanoparticle formulation was cleaned two times with pure ethanol. After cleaning, the polyA tubing was washed with mQ water and tubing for lipid solutions with pure ethanol.

A total of 2 litres of 1x PBS was prepared and two dialysis cassettes (Slide-A-Lyzer™ 10K MWCO) with 3 ml capacity were hydrated according to the manufacturer's instructions.

Immediately prior to microfluidic injection, the polyA solution was diluted to required concentration in 25 mM sodium acetate and loaded into a 20 ml syringe. The syringe pump was set to deliver 9 ml/min, corresponding to an injection volume of ~1.8 ml over 12 seconds. Lipid solutions were loaded into a 10 ml syringe on the opposite inlet arm of the microfluidics device and injected at a rate corresponding to 0.6 ml over the same 12 second period. Both syringes were started simultaneously. The initial drop exiting the mixer was discarded and sample collection began immediately thereafter and continued for 12 seconds.

Following LNP formation, a 5 ml syringe containing 2 ml of air was used to introduce oxygen into the dialysis membrane. The membrane was punctured from the top corner carefully and air was injected, followed by LNP suspension. The volume of LNPs loaded into the membrane was recorded. Samples were dialyzed against 1x DPBS at 4 °C overnight under gentle stirring (140 RPM).

On the following day, the dialysis membrane was punctured with a 5 ml syringe preloaded with 2 ml of air to allow displacement of the internal volume. The LNP-containing solution was collected, and the recovered volume was recorded. To remove residual buffer components and concentrate the nanoparticles, samples were washed using Amicon® ultra centrifugal filters (15kDa MWCO). Centrifugation was performed in Eppendorf 5810 R centrifuge at 3000*g* for 10 minutes 3 times.

The amount of peptide required for conjugation was calculated based on a threefold molar excess relative to the reactive lipid component. The appropriate volume of peptide was diluted in 1X DPBS and added directly to the LNP suspension. The mixture was incubated for 2 hours at room temperature under gentle end-over end rotation to facilitate the conjugation reaction. The peptides used were RPAR, long Cerepep and their "scrambled" versions, where the aminoacid sequence was randomised.

Following incubation, the samples were transferred into sterile glass vials and stored at 4 °C until further use.

The same process described above was performed for encapsulating Cre mRNA into LNPs. CleanCap® Cre mRNA was obtained from Trilink, USA (cat. no. L-7211) and used at a target concentration of 111 µg/ml.

2.3 Results

2.3.1 NRP1 expression profiling in candidate cell lines

Western blot analysis was performed to compare Neuropilin 1 (NRP1) expression across selected cell lines and to guide the selection of models for subsequent testing of RPAR functionalised LNPs. In addition to PPC1 and M21 cells, DU145 and Neuro2a were included to determine whether RPAR-LNPs should also be evaluated in cell lines showing detectable, but potentially less abundant receptor expression.

Strong NRP1 signal was observed in PPC1, DU145 and Neuro2a cells, while M21 cells showed no detectable expression (Figure 4). This supported the inclusion of DU145 cells in subsequent evaluation of RPAR-functionalised LNPs, as it may represent a model with less abundant and potentially more physiologically relevant receptor expression than PPC1. Together, these results supported the use of multiple cell lines with differing apparent NRP1 expression levels for evaluating RPAR-mediated delivery.

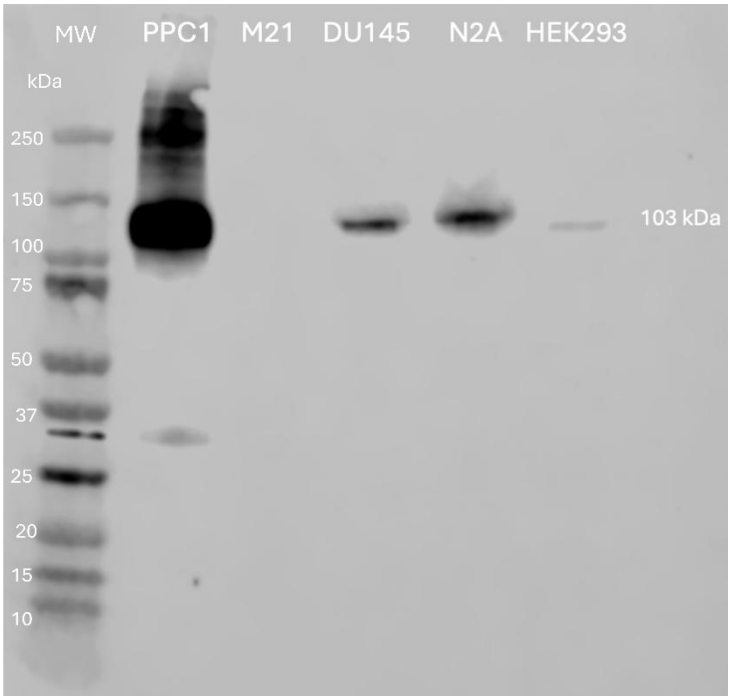

Figure 4. Western blot analysis of NRP1 expression in PPC1, M21, DU145, Neuro2a and HEK293 cell lines.

2.3.2 Evaluation of VP1-mediated plasmid transfection efficiency

To further evaluate transfection efficiency, Neuro2a, PPC1, DU145 and GL261 cells were transfected using VP1 reagent in combination with a dual DsRed2/eGFP plasmid.

At 24 h post transfection, detectable fluorescence signal was observed in several tested VP1 transfected cell lines (Figure 5). In PPC1 cells, fluorescent signal was detected at both CR2.5 and CR3 conditions (Figure 5A). The CR3 samples demonstrated visibly stronger fluorescence intensity and a larger number of fluorescent cells compared to CR2.5 samples, indicating improved transfection efficiency at higher charge ratios. Fluorescent cells were distributed unevenly throughout the field of view, with some clusters showing stronger signal intensity.

In the case of DU145 cells, fluorescence was observed at both CR1.5 and CR3 conditions (Figure 5B). CR3 condition appeared to produce a more intense fluorescence signal and a greater number of fluorescent cells that CR1.5, indicating increased transfection efficiency at the higher charge ratio.

GL261 cells also showed detectable fluorescence at both CR1.5 and CR3 conditions (Figure 5C). CR1.5 samples showed sparse fluorescent cells and weaker overall signal intensity. In comparison, GL261 CR3 samples exhibited stronger fluorescence distributed across a larger proportion of the imaged field.

Among the VP1 treated samples, Neuro2a cells demonstrated the most extensive fluorescence across multiple charge ratios. Fluorescence was detectable at all charge ratios (CR1.5-CR3, Figure 5D). Increasing charge ratio generally corresponded with increased fluorescence intensity and a higher apparent number of fluorescent cells. The strongest fluorescence signal was observed at CR3 samples, where multiple fluorescent cells and brighter signal distribution were visible across several independent images. Among all VP1 transfected samples, N2a CR3 conditions demonstrated some of the highest apparent fluorescence intensity.

At 48 h post transfection, fluorescence remained detectable in VP1 transfected PPC1 cells (Figure 5A). PPC1 CR2.5 samples showed moderate fluorescence signal, while PPC1 CR3 samples demonstrated strong fluorescence with several brightly fluorescent cells visible throughout the field of view. Compared to the corresponding 24 h images, fluorescence signal at 48 h appeared more pronounced and widespread, suggesting increased pDNA expression over time.

Limited 48h VP1 images were available for Neuro2a CR1.5 samples (Figure 5D). These images showed little detectable fluorescence compared to higher charge ratio conditions, indicating that this CR was insufficient for this cell line.

Overall, VP1 mediated transfection resulted in detectable fluorescence in all tested cell lines, with higher charge ratios generally associated with stronger fluorescence signal and increased apparent transfection efficiency.

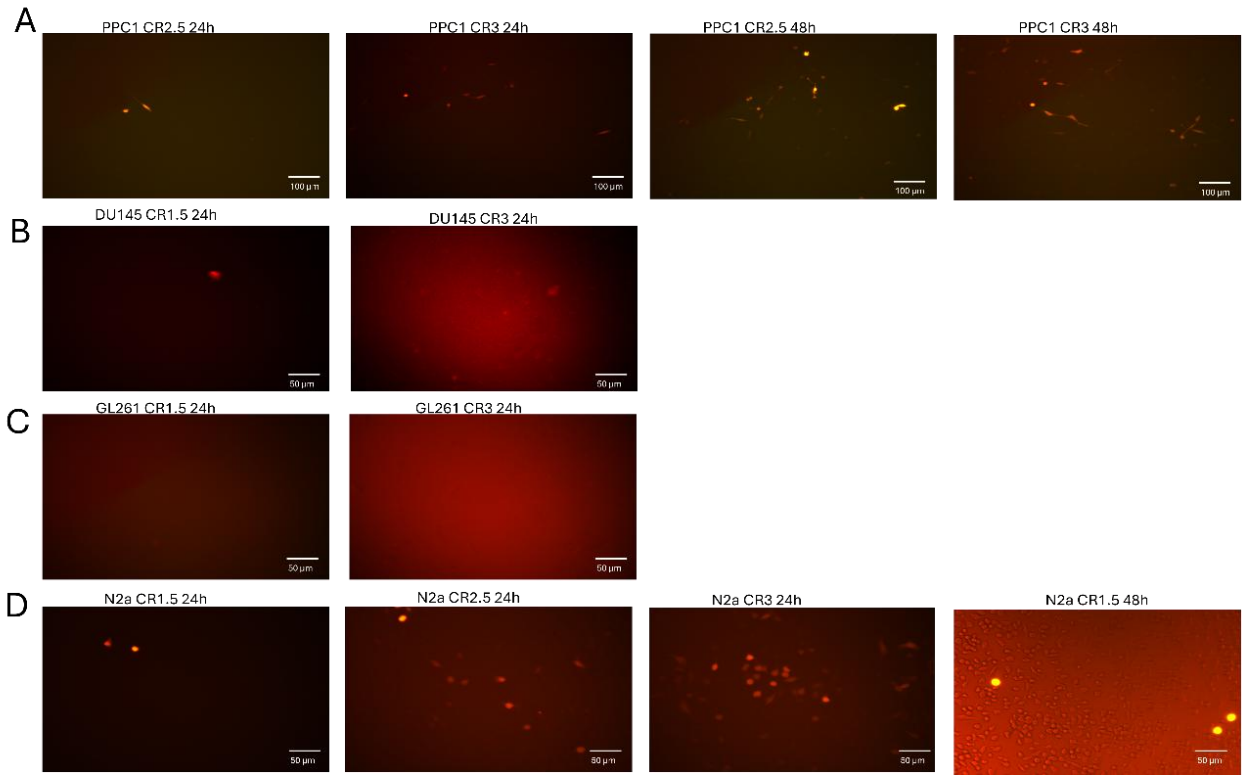

Figure 5. Fluorescence microscopy images of VP1-mediated pDNA transfection in Neuro2a, PPC1, DU145 and GL261 cells at different charge ratios and time points. Fluorescence microscopy images showed reporter expression following VP1-mediated transfection using the dual Ai9/eGFP plasmid. A) PPC1 cells 24 h and 48 h post-transfection; B) DU145 cells at 24h post-transfection C) GL261 cells at 24h post-transfection D) Neuro2a cells 24 h and 48 h post-transfection. Images were acquired using 10x and 20x magnification. Scale bars: 100 µm (10x) and 50 µm (20x).

2.3.3 Evaluation of VP4-mediated plasmid transfection efficiency

To evaluate the efficiency of pDNA delivery with a second transfection reagent, VP4, three cell lines (Neuro2a, PPC1 and DU145) were used. Under initial conditions (500 ng pDNA per well), the strongest fluorescence signal was observed in Neuro2a cells, as indicated by detectable fluorescence signal in microscopy images (Figure 6).

At 24 h post transfection, Neuro2a cells transfected with VP4 demonstrated detectable fluorescence at all tested charge ratios (CR1.5-CR3, Figure 6A). CR1.5 samples displayed

relatively weak fluorescence signal with only a small number of fluorescent cells visible. Increasing the charge ratio to CR2 resulted in brighter fluorescence intensity and an increased number of fluorescent cells. Further increases to CR2.5 and CR3 produced progressively stronger and more widespread fluorescence throughout the field of view. Among the VP4-transfected Neuro2a samples, CR3 condition demonstrated the strongest fluorescence signal. Multiple brightly fluorescent cells were visible across several independent images at both magnifications, suggesting increased apparent transfection efficiency compared to lower charge ratios. Fluorescence was distributed across a larger proportion of the field at CR3 conditions.

In addition, Neuro2a CR3 samples demonstrated at 48 h post transfection clear and sustained fluorescence signal (Figure 6B), indicating continued plasmid expression at the later time point. Compared to the corresponding 24 h images, fluorescence at 48 h remained detectable or slightly increased.

At 48 h post-transfection, VP4 transfected PPC1 cells demonstrated detectable fluorescence at CR2, CR2.5 and CR3 (Figure 6C). Fluorescence intensity appeared moderate at CR2 and CR2.5 conditions, but strongest at CR3 dose. In addition, VP4-transfected Neuro2a CR3 samples at 48 h demonstrated clear fluorescence signal, suggesting sustained plasmid expression over time. DU145 cells did not produce any fluorescent signal upon transfection with VP4-pDNA complexes.

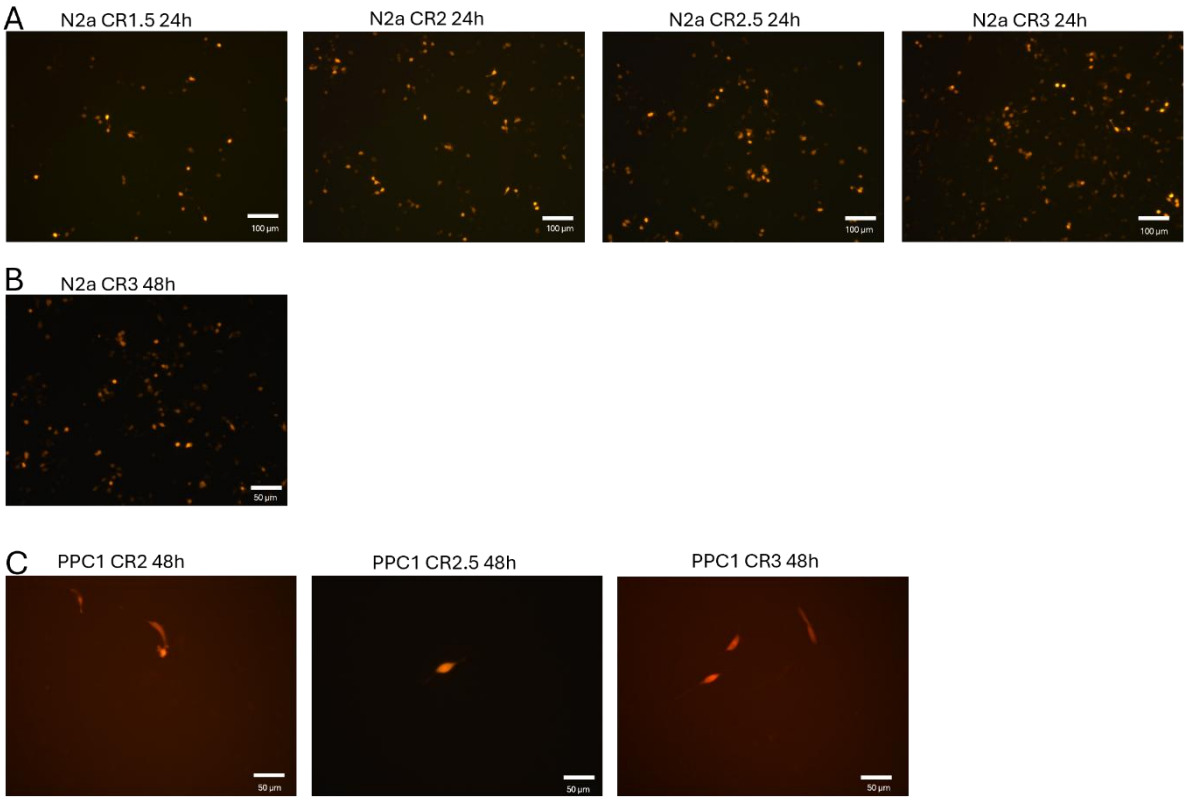

Figure 6. Fluorescence microscopy images of VP4-mediated pDNA transfection in Neuro2a, DU145 and PPC1 cells at different charge ratios and time points. Images show fluorescence signal following VP4-mediated plasmid delivery with differences in signal intensity and number of cells observed between charge ratios and time points. A) Neuro2a cells 24h post-transfection; B) Neuro2a cells 48h post-transfection; C) PPC1 cells 48h post-transfection. Images were acquired using 10x and 20x magnification. Scale bars: 100 μm (10x) and 50 μm (20x).

2.3.4 Brain-targeted LNP-mediated mRNA delivery in cultured cells

The ability of LNPs functionalized with a TPPs to deliver nucleic acid cargo was evaluated in Neuro2a and PPC1 cells using fluorescence microscopy. LNP formulations were conjugated either to the following TPPs (obtained from TAG Copenhagen, Denmark): brain-specific TPP long Cerepep (longCP) and its scrambled version (both sequences are proprietary), or lung-specific TPP RPAR (Acetyl-Cysteine-Ahx-RPARPAR-OH) or scrambled (Acetyl-Cysteine-Ahx-RRAAPRP-OH) and incubated with cells for 1h. Reporter activation was determined in both GFP and RFP fluorescence channels at 1, 24 and 48h after incubation with Cre mRNA containing LNPs.

At a 1-hour mark after incubation with LNPs, green (from LNP uptake) and yellow fluorescence signal was observed in multiple conditions, although signal intensity varied between formulations (Figure 7). In Neuro2a cells treated with VP4-mediated LNP formulations, unconjugated CR1.5 LNPs produced relatively weak fluorescence signal, whereas peptide-functionalised formulations demonstrated stronger fluorescence and a greater apparent number of fluorescent cells. Among these conditions, VP4 CR3 longCP LNPs produced the strongest fluorescence signal in both GFP and red channels, indicating successful intracellular delivery and reporter activation (Figure 7A-B). In Neuro2a cells CR3 longCP LNPs demonstrated stronger fluorescence compared with CR2.5 scrLongCP conditions (Figure 7C-D).

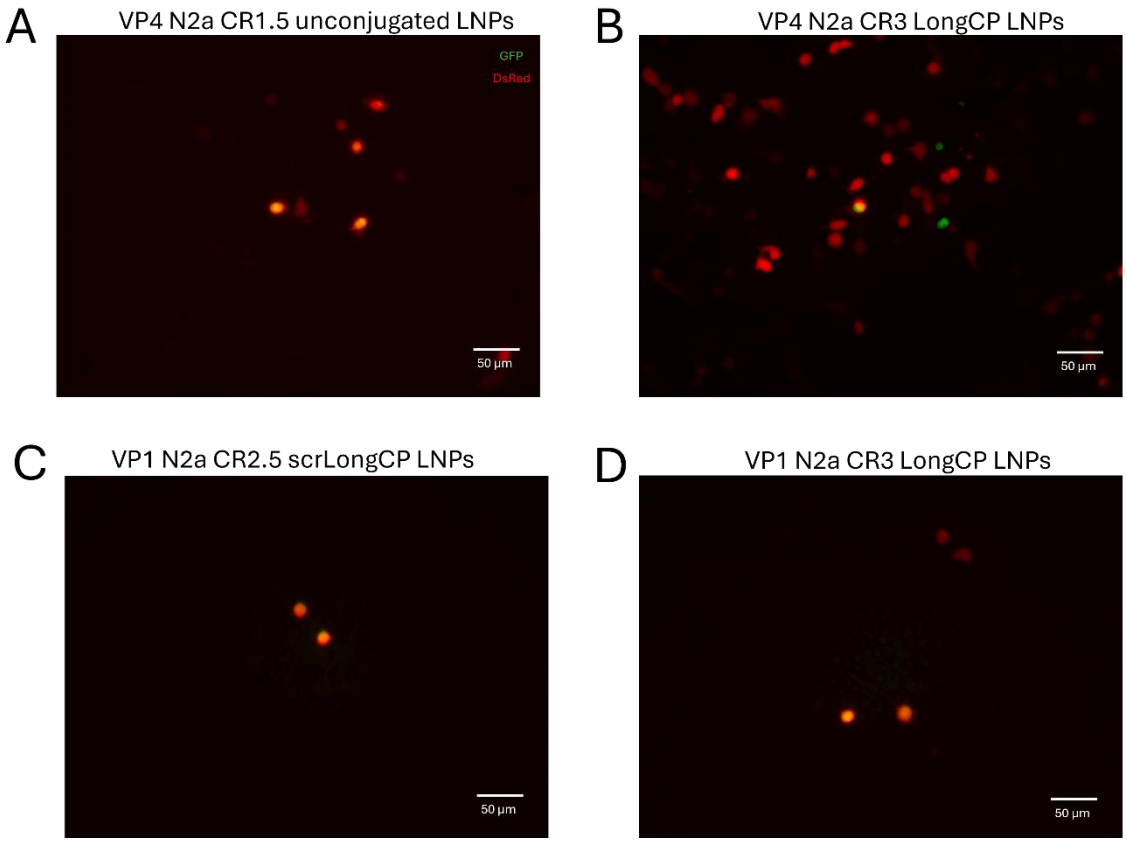

Figure 7. Early reporter cell activation following LNP-mediated delivery of Cre mRNA in Neuro2a cells 1 h after treatment. Fluorescence microscopy images showed reporter activation following treatment with VP1- and VP4-mediated peptide-functionalised LNP formulations. A-B) Neuro2a cells treated with VP4 CR1.5 unconjugated and V4 CR3 longCP LNPs; C-D) Neuro2a cells treated with VP1 CR2.5 scrLongCP and VP1 CR3 longCP LNPs. Images were acquired 1 h after exposure to Cre mRNA-containing LNPs. Images were acquired 20x magnification.

At 24 h after exposure, fluorescence signal remained detectable across multiple formulations (Figure 8). In Neuro2a cells, VP4 CR3 longCP LNPs demonstrated strong and sustained fluorescence signal in both GFP and red channels (Figure 8C). Compared to lower charge ratio and scrambled conditions, CR3 longCP formulations produced brighter fluorescence throughout the field of view (Figure 8A-C).

VP1-mediated LNP delivery similarly resulted in detectable fluorescence at 24 h with CR3 longCP LNPs again producing stronger fluorescence signal than CR2.5 scrLongCP formulations (Figure 8D-E). In PPC1 cells there was very little fluorescence detected in CR 3 RPAR LNPs (Figure 8F).

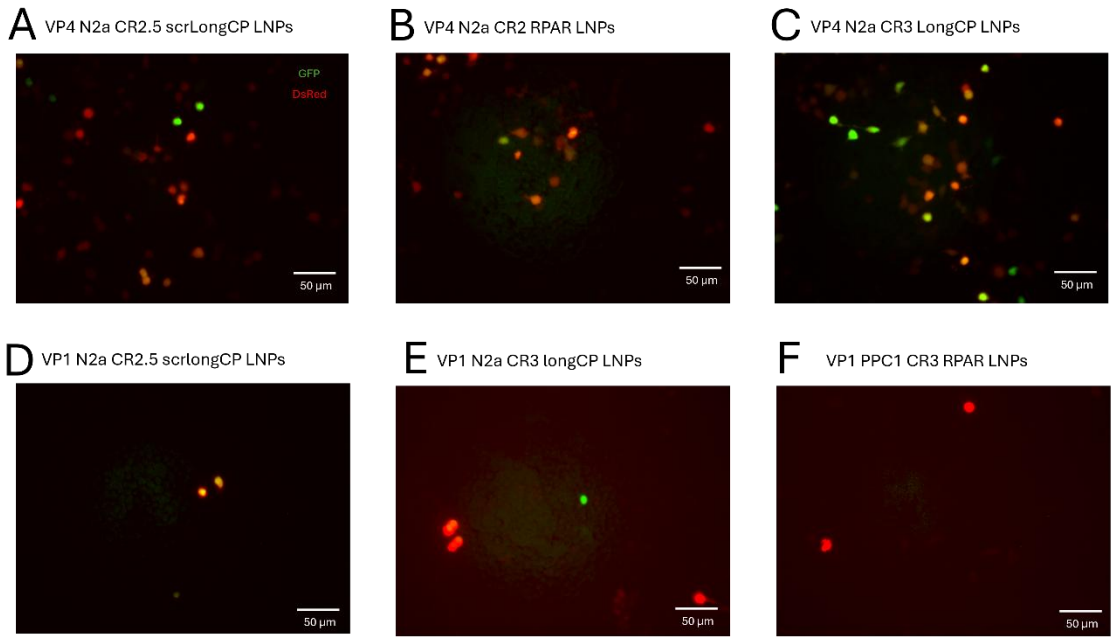

Figure 8. Sustained reporter activation following LNP-mediated delivery of Cre mRNA in Neuro-2a cells 24 h after treatment. Fluorescence microscopy images showed reporter activation following treatment with VP4- and VP1-mediated peptide-functionalised LNPs. A-C) Neuro2a cells treated with VP4 CR2.5 scrLongCP, VP4 CR2 RPAR and VP4 CR3 longCP LNPs; D-F) Neuro2a cells treated with VP1 CR2.5 scrLongCP, VP1 CR3 longCP LNPs and VP1 CR3 RPAR LNPs. Images were acquired 24 h after exposure to Cre mRNA-containing LNPs. Images were acquired using 20x magnification.

At 48 h after exposure, fluorescence signal remained detectable in both VP1- and VP4-mediated LNP formulations, indicating sustained reporter activation over time (Figure 9). In Neuro2a cells treated with VP4-mediated formulations, unconjugated CR 1.5 LNPs continued to demonstrate relatively weak fluorescence signal, whereas VP4 CR3 longCp LNPs produced the strongest and most widespread fluorescence signal among the tested conditions (Figure 9A-D). VP4 CR2 RPAR LNPs and CR2.5 scrLongCP LNPs demonstrated detectable fluorescence, although signal intensity appeared lower than in VP4 CR3 longCP samples.

VP1-mediated LNP formulations similarly demonstrated sustained fluorescence signal at 48 h post treatment (Figure 9). In Neuro2a cells, VP1 CR3 longCP formulations showed detectable fluorescence (Figure 9E). In PPC1 cells, VP1 CR3 unconjugated formulations demonstrated detectable fluorescence signal in both GFP and red channels at 48 h post treatment (Figure 9F).

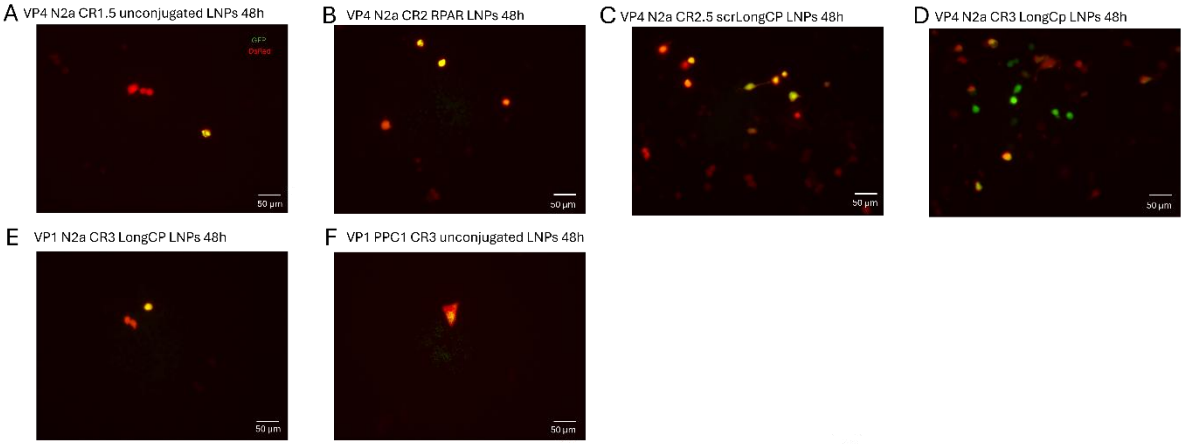

Figure 9. Sustained reporter activation following LNP-mediated delivery of Cre mRNA in Neuro2a and PPC1 cells 48 h after treatment. Fluorescence microscopy images showed reporter activation following treatment with VP1- and VP4-mediated peptide functionalised LNPs. A–D) Neuro2a cells treated with VP4 CR1.5 unconjugated, VP4 CR2 RPAR, VP4 CR2.5 scrLongCP and VP4 CR3 longCP LNPs; E–F) Neuro2a cells treated with VP1 CR2.5 scrLongCP and VP1 CR3 longCP LNPs; G) PPC1 cells treated with VP1 CR3 unconjugated LNPs. Images were acquired 48 h after exposure to Cre mRNA-containing LNPs. Images were acquired using 20x magnification.

Overall, fluorescence microscopy analysis demonstrated successful reporter activation following LNP-mediated delivery in both Neuro2a and PPC1 cells. Higher charge ratios and peptide-functionalised formulations, particularly VP4 CR3 longCP LNPs, consistently produced the strongest fluorescence signal across multiple time points.

2.3.5 Quantification of LNP-mediated reporter activation using flow cytometry

Flow cytometry was used to evaluate Cre-mediated reporter activation after LNP delivery in VP4-transfected Neuro2a cells (Figure 10). Cells were first transfected with plasmid DNA encapsulated in VP4; this transfection resulted in red fluorescence in transfected cells, detectable in the FL2-A channel. 48h after the transfection, cells were incubated for 1 hour with longCP-conjugated LNPs containing Cre mRNA, and fluorescence was analysed in both the FL2-A (red) and FL1-A (green) channels.

Mean FL2-A values showed 4.3x times higher red fluorescent signal in transfected cells vs. untreated cell sample (Figure 10A,C). However, incubation with LNPs resulted in the 5.8x higher mean FL1-A value in comparison to untreated cells. These results indicate successful delivery of functional Cre mRNA by longCP-conjugated LNPs and activation of reporter switching in the Ai9 system. (Figure 10B,C).

A

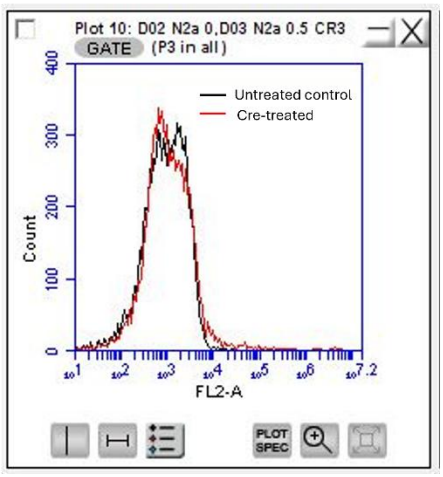

B

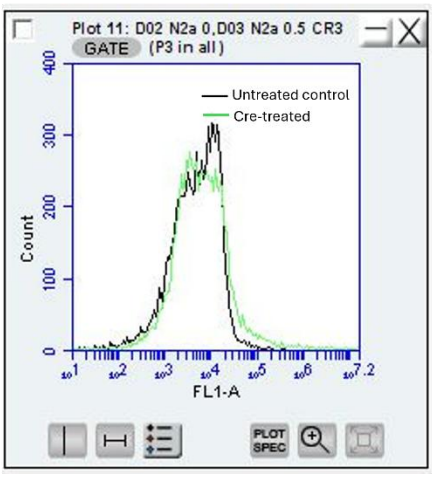

C

Plot 10: Multiple Samples Gated on (P3 in all)	Count	Volume (µL)	% of This Plot	% of All	Mean FL2-A	CV FL2-A	Median FL2-A
D02 N2a 0 : This Plot	10 000	87	100,00%	12,71%	1 281,07	99,69%	
D03 N2a 0.5 CR3 : This Plot	10 000	69	100,00%	15,76%	5 562,52	1 969,45%	

Plot 11: Multiple Samples Gated on (P3 in all)	Count	Volume (µL)	% of This Plot	% of All	Mean FL1-A	CV FL1-A	Median FL1-A
D02 N2a 0 : This Plot	10 000	87	100,00%	12,71%	7 537,32	142,48%	
D03 N2a 0.5 CR3 : This Plot	10 000	69	100,00%	15,76%	44 080,10	1 107,35%	

Figure 10. Flow cytometry analysis of Cre-mediated reporter activation in VP4-transfected Neuro2a cells following treatment with longCP conjugated LNPs containing Cre mRNA. Histograms show FL2-A red fluorescence distribution (A) and FL1-A green fluorescence distribution (B) in untreated control and Cre-treated cells. A rightward shift in green fluorescence intensity is observed in Cre-treated cells. Quantitative summary of flow cytometry data showing cell count (C), analysed volume, mean fluorescence intensity and coefficient of variation (CV) for untreated and Cre-treated samples in FL2-A and FL1-A channels.

2.4 Discussion

The aim of this study was to evaluate non-viral gene delivery strategies, including CPP-based transfection and LNP-mediated delivery, using Cre/Ai9 reporter system as a functional readout of delivery efficiency. Overall, both CPP-mediated transfection and LNP-mediated delivery indicated detectable reporter activation in several tested cell lines, although fluorescence intensity varied between delivery systems, charge ratios, LNP formulations and cell types. These findings support the usefulness of reporter-based assays for evaluating functional intracellular delivery, since reporter activation reflects not only cellular uptake, but also successful cargo release and biological activity inside the cell (Cheng et al., 2020; Vasudevan et al., 2025).

Both VP1- and VP4-mediated transfection resulted in detectable fluorescence in multiple cell lines, with higher charge ratios generally producing stronger fluorescence signals (Figures 5-6). Neuro2a cells demonstrated the strongest apparent reporter activation, particularly under CR3 conditions, while PPC1 cells also showed clear fluorescence at higher charge ratios. In

comparison, DU145 and GL261 cells often showed weaker or more sparse fluorescence (Figures 5-6). These observations suggest that both VP1 and VP4 can support functional plasmid delivery, but that delivery efficiency depends strongly on cellular context and transfection conditions.

The stronger fluorescence observed at higher charge ratios may be explained by improved formation of peptide-DNA complexes. CPP-mediated plasmid delivery depends on electrostatic interactions between positively charged peptides and negatively charged DNA, which can enhance cellular uptake and protect the cargo from degradation (Guidotti et al., 2017). Therefore, increasing the charge ratio may improve complex formation and interaction with the cell membrane. However, this interpretation should be made cautiously, because very high positive charge can also increase aggregation or cytotoxicity. Since cell viability was not assessed together with fluorescence in this study, the strongest fluorescence condition cannot automatically be considered the optimal delivery condition.

Cell-line-dependent differences were observed throughout the CPP-mediated transfection experiments. Neuro2a cells consistently demonstrated stronger fluorescence after both CPP-mediated transfection and LNP-mediated delivery, whereas several DU145 and GL261 conditions produced weaker fluorescence signals. These differences may reflect variation in membrane composition, proliferation rate, endocytic activity or intracellular trafficking between cell lines. This is consistent with previous findings showing that CPP uptake mechanisms can vary depending on the peptide, cargo and experimental conditions (Bechara & Sagan, 2013; Guidotti et al., 2017).

The LNP-mediated delivery experiments showed that peptide-functionalised LNPs were able to induce detectable reporter activation in Neuro2a and PPC1 cells (Figures 7-9). Among the tested conditions, VP4 CR3 longCP-functionalised LNPs produced the strongest and most widespread fluorescence signal, especially in Neuro2a cells at 48 hours. Fluorescence was also detectable RPAR-functionalised, scrambled peptide and unconjugated LNP conditions, although the signal intensity varied between them. These results suggest that both charge ratio and surface functionalisation influenced apparent delivery efficiency.

The stronger signal observed with longCP-functionalised LNPs may indicate that peptide functionalisation improved cell association, uptake or intracellular delivery. Surface functionalisation with targeting ligands can improve selective delivery and reduce off-target exposure, which is one of the main reasons targeted LNP systems are being developed (Tang et al., 2023). The approximately 10-fold increase in FL1-A fluorescence observed after treatment with longCP LNPs containing Cre mRNA further successful intracellular delivery and

functional Cre-mediated recombination (Figure 10C). Importantly, this fluorescence switch demonstrates not only cellular uptake of LNP cargo but also successful cytosolic release and biological activity of the delivered mRNA. Because TPPs can promote cellular uptake and tissue penetration through receptor-mediated mechanisms, the stronger fluorescence observed with longCP-functionalised formulations may reflect improved intracellular transport efficiency. This interpretation is consistent with previous studies demonstrating enhanced delivery using peptide-functionalised nanoparticle systems (Sugahara et al., 2009, 2010; Teesalu et al., 2012).

The sustained fluorescence observed at 24 and 48 hours after LNP exposure suggests that the delivered cargo was able to produce a functional reporter response over time. This is important because cellular uptake alone does not guarantee successful functional delivery. After internalisation, LNP cargo can remain trapped in endosomes, be recycled out of the cell or be degraded before reaching the cytosol (Sahay et al., 2013). Therefore, reporter activation provides a more informative readout than nanoparticle uptake alone, because it indicates that the delivered nucleic acid cargo produced a biological effect inside the cell.

The Cre reporter system was useful in this study because RFP expression depends on successful intracellular delivery and activity of Cre recombinase. As a result, fluorescence activation reflects functional delivery rather than simple nanoparticle association with the cell surface. This is particularly relevant for both LNP- and CPP-mediated delivery systems, where intracellular release and biological activity are often more limiting than initial cellular uptake.

Several limitations should be considered when interpreting these results. Most microscopy-based analyses were qualitative and relied on visual comparison of fluorescence intensity and apparent numbers of fluorescent cells. Quantitative image analysis, determination of the percentage of fluorescent cells and measurement of mean fluorescence intensity would improve the reliability of comparisons between charge ratios, peptides and LNP formulations. In addition, several experimental variables changed simultaneously between conditions, including peptide type, charge ratio, LNP functionalization and cell line, making it difficult to determine the precise contribution of each factor. Finally, cell viability was not assessed together with delivery efficiency, although this would be important for evaluating the biological suitability of highly fluorescent conditions.

In conclusion, this study shows that both CPP-based and LNP-mediated delivery strategies can concentration-dependently activate reporter expression in vitro. Higher charge ratios generally produced stronger apparent reporter activation, especially in Neuro2a and PPC1 cells. Among the tested LNP conditions, VP4 CR3 longCP-functionalised LNPs produced the strongest

microscopy-based fluorescence signal. Overall, the results suggest that delivery efficiency depends strongly on formulation, charge ratio and cell type, and that the Ai9/Cre reporter system is a useful tool for evaluating functional intracellular delivery.

Conclusion

This study evaluated non-viral delivery strategies using CPP-mediated transfection and peptide-functionalised LNPs in combination with Cre/Ai9 reporter system. Both VP1- and VP4-mediated transfections resulted i detectable reporter activation in several tested cell lines, demonstrating successful plasmid delivery and expression. In general, higher charge ratios produced stronger fluorescence signal, with Neuro2a and PPC1 cells showing the highest apparent transfection efficiency. Among the tested CPP formulations, CR3 conditions consistently produced the strongest reporter activation.

LNP-mediated delivery experiments demonstrated that peptide-functionalised LNPs could deliver functional Cre mRNA and inducing reporter activation in Neuro2a and PPC1 cells. longCP functionalised formulations, particularly VP4 CR3 longCP LNPs, produced the strongest and most sustained fluorescence signal across multiple time points. In contrast, unconjugated and scrambled peptide formulations generally resulted in weaker fluorescence. These findings suggest that both charge ratio and peptide functionalisation influence apparent delivery efficiency.

Overall, the results demonstrate that Cre/Ai9 reporter system is a useful tool for evaluating functional intracellular delivery of nucleic acid cargo. The findings further suggest that CPP-mediated transfection and peptide-functionalised LNP systems represent promising non-viral delivery approaches for future delivery applications. However, additional quantitative analysis and optimisation of formulation parameters will be necessary to further improve delivery efficiency and evaluate the broader applicability of these systems.

RESÜMEE

Lipiidsete nanoosakeste vahendatud Cre mRNA kohaletoimetamise efektiivsuse hindamine erinevates vähirakkude liinides

Berit Hiie

Resümee

Lipiidsed nanoosakesed (LNP-d) ja rakku penetreerivad peptiidid (CPP-d) on viimastel aastatel kujunenud paljulubavateks mitteviiruslike geeniedastuse meetodiks, võimaldades transportida rakkudesse erinevaid nukleiinhappeid (Hou et al., 2021). Võrreldes viirusvektoritega on mitteviiruslikel süsteemidel mitmeid eeliseid, nagu parem ohutusprofiil, väiksem immunogeensus ja lihtsam tootmine (Cullis & Hope, 2017). Samal ajal on efektiivne rakusisene kohaletoimetamine endiselt keeruline, kuna nukleiinhapped peavad pärast raku poolt omastamist vältima endosomaalset degradatsiooni ja säilitama oma bioloogilise aktiivsuse (Sahay et al., 2013). Üheks võimalikuks lahenduseks on rakku penetreerivate peptiidide (CPP-de) ja peptiid-funktsionaliseeritud LNP-de kasutamine, mis võivad parandada nukleiinhapete rakulist omastamist ja rakusisest transporti (Guidotti et al., 2017; Sugahara et al., 2009).

Käesoleva bakalaureusetöö eesmärk oli hinnata mitteviirusliku geeniedastuse efektiivsust CPP-põhiste transfektsioonisüsteemide ja peptiid-funktsionaliseeritud LNP-de abil erinevates vähirakkude liinides. Töö käigus uuriti VP1- ja VP4-põhiste transfektsioonireagentide võimet vahendada plasmiidse DNA rakusisest kohaletoimetamist Neuro2a, PPC1, DU145 ja GL261 rakkudes. Lisaks hinnati longCP-, RPAR- ja scrambled peptiididega funktsionaliseeritud LNP-de võimet transportida Cre mRNA-d rakkudesse ning aktiveerida Cre/Ai9 reportersüsteemi. Reporteraktivatsiooni hinnati fluorestsentsmikroskoopia ja läbivoolu tsütomeetria abil.

Tulemused näitasid, et nii VP1- kui ka VP4 vahendatud transfektsioon võimaldas reportersignaali aktivatsiooni mitmes rakuliinis. Üldiselt põhjustasid kõrgemad laengusuhted tugevama fluorestsentsi ning kõige tugevamat signaali täheldati Neuro2a rakkudes. LNP vahendatud transpordi katsed näitasid, et peptiid-funktsionaliseeritud LNP-d suutsid edukalt vahendada funktsionaalse Cre mRNA rakusisest kohaletoimetamist. Kõige tugevam ja püsivam fluorestsents täheldati VP4 CR3 longCP LNP-de puhul, samas kui scrambled peptiidide ja funktsionaliseerimata LNP-de puhul oli signaal üldiselt nõrgem.

Kokkuvõttes näitas käesolev bakalaureusetöö, et nii CPP põhised transfektsioonisüsteemid kui ka peptiid-funktsionaliseeritud LNP-d on paljulubavad mitteviiruslikud geeniedastuse meetodid. Lisaks kinnitaisd tulemused, et Cre/Ai9 reportersüsteem võimaldab efektiivselt hinnata funktsionaalset rakusisest kohaletoimetamist erinevates rakuliinides.

Bibliography

Alshehry, Y., Liu, X., Li, W., Wang, Q., Cole, J., & Zhu, G. (2025). Lipid Nanoparticles for mRNA Delivery in Cancer Immunotherapy. *The AAPS Journal*, *27*(3), 66. https://doi.org/10.1208/s12248-025-01051-8

Bechara, C., & Sagan, S. (2013). Cell-penetrating peptides: 20 years later, where do we stand? *FEBS Letters*, *587*(12), 1693–1702. https://doi.org/10.1016/j.febslet.2013.04.031

Blanco, E., Shen, H., & Ferrari, M. (2015). Principles of nanoparticle design for overcoming biological barriers to drug delivery. *Nature Biotechnology*, *33*(9), 941–951. https://doi.org/10.1038/nbt.3330

Brooks, P. C., Montgomery, A. M. P., Rosenfeld, M., Reisfeld, R. A., Hu, T., Klier, G., & Cheresh, D. A. (1994). Integrin αvβ3 antagonists promote tumor regression by inducing apoptosis of angiogenic blood vessels. *Cell*, *79*(7), 1157–1164. https://doi.org/10.1016/0092-8674(94)90007-8

Brothman, A. R., Lesho, L. J., Somers, K. D., Wright, G. L., & Merchant, D. J. (1989). Phenotypic and cytogenetic characterization of a cell line derived from primary prostatic carcinoma. *International Journal of Cancer*, *44*(5), 898–903. https://doi.org/10.1002/ijc.2910440525

Cheng, Q., Wei, T., Farbiak, L., Johnson, L. T., Dilliard, S. A., & Siegwart, D. J. (2020). Selective organ targeting (SORT) nanoparticles for tissue-specific mRNA delivery and CRISPR–Cas gene editing. *Nature Nanotechnology*, *15*(4), 313–320. https://doi.org/10.1038/s41565-020-0669-6

Cullis, P. R., & Hope, M. J. (2017). Lipid Nanoparticle Systems for Enabling Gene Therapies. *Molecular Therapy*, *25*(7), 1467–1475. https://doi.org/10.1016/j.ymthe.2017.03.013

D'Astolfo, D. S., Pagliero, R. J., Pras, A., Karthaus, W. R., Clevers, H., Prasad, V., Lebbink, R. J., Rehmann, H., & Geijsen, N. (2015). Efficient Intracellular Delivery of Native Proteins. *Cell*, *161*(3), 674–690. https://doi.org/10.1016/j.cell.2015.03.028

Erazo-Oliveras, A., Najjar, K., Dayani, L., Wang, T.-Y., Johnson, G. A., & Pellois, J.-P. (2014). Protein delivery into live cells by incubation with an endosomolytic agent. *Nature Methods*, *11*(8), 861–867. https://doi.org/10.1038/nmeth.2998

Eygeris, Y., Gupta, M., Kim, J., & Sahay, G. (2022). Chemistry of Lipid Nanoparticles for RNA Delivery. *Accounts of Chemical Research*, *55*(1), 2–12. https://doi.org/10.1021/acs.accounts.1c00544

Eygeris, Y., Patel, S., Jozic, A., & Sahay, G. (2020). Deconvoluting Lipid Nanoparticle Structure for Messenger RNA Delivery. *Nano Letters*, *20*(6), 4543–4549. https://doi.org/10.1021/acs.nanolett.0c01386

Guidotti, G., Brambilla, L., & Rossi, D. (2017). Cell-Penetrating Peptides: From Basic Research to Clinics. *Trends in Pharmacological Sciences*, *38*(4), 406–424. https://doi.org/10.1016/j.tips.2017.01.003

Hoess, R. H., Ziese, M., & Sternberg, N. (1982). P1 site-specific recombination: Nucleotide sequence of the recombining sites. *Proceedings of the National Academy of Sciences*, *79*(11), 3398–3402. https://doi.org/10.1073/pnas.79.11.3398

Hou, X., Zaks, T., Langer, R., & Dong, Y. (2021). Lipid nanoparticles for mRNA delivery. *Nature Reviews Materials*, *6*(12), 1078–1094. https://doi.org/10.1038/s41578-021-00358-0

Jain, R. K. (2013). Normalizing Tumor Microenvironment to Treat Cancer: Bench to Bedside to Biomarkers. *Journal of Clinical Oncology*, *31*(17), 2205–2218. https://doi.org/10.1200/JCO.2012.46.3653

Kulkarni, J. A., Darjuan, M. M., Mercer, J. E., Chen, S., Van Der Meel, R., Thewalt, J. L., Tam, Y. Y. C., & Cullis, P. R. (2018). On the Formation and Morphology of Lipid

Nanoparticles Containing Ionizable Cationic Lipids and siRNA. *ACS Nano*, *12*(5), 4787–4795. https://doi.org/10.1021/acsnano.8b01516

Kulkarni, J. A., Witzigmann, D., Leung, J., Tam, Y. Y. C., & Cullis, P. R. (2019). On the role of helper lipids in lipid nanoparticle formulations of siRNA. *Nanoscale*, *11*(45), 21733–21739. https://doi.org/10.1039/C9NR09347H

Madisen, L., Mao, T., Koch, H., Zhuo, J., Berenyi, A., Fujisawa, S., Hsu, Y.-W. A., Garcia, A. J., Gu, X., Zanella, S., Kidney, J., Gu, H., Mao, Y., Hooks, B. M., Boyden, E. S., Buzsáki, G., Ramirez, J. M., Jones, A. R., Svoboda, K., … Zeng, H. (2012). A toolbox of Cre-dependent optogenetic transgenic mice for light-induced activation and silencing. *Nature Neuroscience*, *15*(5), 793–802. https://doi.org/10.1038/nn.3078

Madisen, L., Zwingman, T. A., Sunkin, S. M., Oh, S. W., Zariwala, H. A., Gu, H., Ng, L. L., Palmiter, R. D., Hawrylycz, M. J., Jones, A. R., Lein, E. S., & Zeng, H. (2010). A robust and high-throughput Cre reporting and characterization system for the whole mouse brain. *Nature Neuroscience*, *13*(1), 133–140. https://doi.org/10.1038/nn.2467

Olmsted, J. B., Carlson, K., Klebe, R., Ruddle, F., & Rosenbaum, J. (1970). Isolation of Microtubule Protein from Cultured Mouse Neuroblastoma Cells. *Proceedings of the National Academy of Sciences*, *65*(1), 129–136. https://doi.org/10.1073/pnas.65.1.129

Porosk, L., Härk, H. H., Arukuusk, P., Haljasorg, U., Peterson, P., & Kurrikoff, K. (2023). The Development of Cell-Penetrating Peptides for Efficient and Selective In Vivo Expression of mRNA in Spleen Tissue. *Pharmaceutics*, *15*(3), 952. https://doi.org/10.3390/pharmaceutics15030952

Sahay, G., Querbes, W., Alabi, C., Eltoukhy, A., Sarkar, S., Zurenko, C., Karagiannis, E., Love, K., Chen, D., Zoncu, R., Buganim, Y., Schroeder, A., Langer, R., & Anderson, D. G. (2013). Efficiency of siRNA delivery by lipid nanoparticles is limited by endocytic recycling. *Nature Biotechnology*, *31*(7), 653–658. https://doi.org/10.1038/nbt.2614

Sauer, B., & Henderson, N. (1988). Site-specific DNA recombination in mammalian cells by the Cre recombinase of bacteriophage P1. *Proceedings of the National Academy of Sciences*, *85*(14), 5166–5170. https://doi.org/10.1073/pnas.85.14.5166

Shaner, N. C., Campbell, R. E., Steinbach, P. A., Giepmans, B. N. G., Palmer, A. E., & Tsien, R. Y. (2004). Improved monomeric red, orange and yellow fluorescent proteins derived from Discosoma sp. Red fluorescent protein. *Nature Biotechnology*, *22*(12), 1567–1572. https://doi.org/10.1038/nbt1037

Stone, K. R., Mickey, D. D., Wunderli, H., Mickey, G. H., & Paulson, D. F. (1978). Isolation of a human prostate carcinoma cell line (DU 145). *International Journal of Cancer*, *21*(3), 274–281. https://doi.org/10.1002/ijc.2910210305

Sugahara, K. N., Teesalu, T., Karmali, P. P., Kotamraju, V. R., Agemy, L., Girard, O. M., Hanahan, D., Mattrey, R. F., & Ruoslahti, E. (2009). Tissue-Penetrating Delivery of Compounds and Nanoparticles into Tumors. *Cancer Cell*, *16*(6), 510–520. https://doi.org/10.1016/j.ccr.2009.10.013

Sugahara, K. N., Teesalu, T., Karmali, P. P., Kotamraju, V. R., Agemy, L., Greenwald, D. R., & Ruoslahti, E. (2010). Coadministration of a Tumor-Penetrating Peptide Enhances the Efficacy of Cancer Drugs. *Science*, *328*(5981), 1031–1035. https://doi.org/10.1126/science.1183057

Szatmári, T., Lumniczky, K., Désaknai, S., Trajcevski, S., Hídvégi, E. J., Hamada, H., & Sáfrány, G. (2006). Detailed characterization of the mouse glioma 261 tumor model for experimental glioblastoma therapy. *Cancer Science*, *97*(6), 546–553. https://doi.org/10.1111/j.1349-7006.2006.00208.x

Tang, X., Zhang, Y., & Han, X. (2023). Ionizable Lipid Nanoparticles for mRNA Delivery. *Advanced NanoBiomed Research*, *3*(8), 2300006. https://doi.org/10.1002/anbr.202300006

Teesalu, Kazuki N Sugahara, & Erkki Ruoslahti. (2012). Mapping of Vascular ZIP Codes by Phage Display. In *Methods in Enzymology* (Vol. 503, pp. 35–56). Elsevier. https://doi.org/10.1016/B978-0-12-396962-0.00002-1

Teesalu, T., Sugahara, K. N., Kotamraju, V. R., & Ruoslahti, E. (2009). C-end rule peptides mediate neuropilin-1-dependent cell, vascular, and tissue penetration. *Proceedings of the National Academy of Sciences*, *106*(38), 16157–16162. https://doi.org/10.1073/pnas.0908201106

Vasudevan, A., Jozić, A., Curtis, A. G., Bodi, E., Ryals, R. C., & Sahay, G. (2025). Lipid nanoparticle-mediated intracameral mRNA delivery facilitates gene expression and editing in the anterior chamber of the eye. *Journal of Controlled Release*, *379*, 1022–1028. https://doi.org/10.1016/j.jconrel.2025.01.068

Vectiopep (n.d.). *Targeted mRNA delivery platform.* Retrived May 14, 2026, from https://vectiopep.ee/

Xu, X., & Xia, T. (2023). Recent Advances in Site-Specific Lipid Nanoparticles for mRNA Delivery. *ACS Nanoscience Au*, *3*(3), 192–203. https://doi.org/10.1021/acsnanoscienceau.2c00062

Zong, Y., Lin, Y., Wei, T., & Cheng, Q. (2023). Lipid Nanoparticle (LNP) Enables mRNA Delivery for Cancer Therapy. *Advanced Materials*, *35*(51), 2303261. https://doi.org/10.1002/adma.202303261

Non-exclusive licence to reproduce the thesis and make the thesis public

I, Berit Hiie

1. grant the University of Tartu a free permit (non-exclusive licence) to

reproduce, for the purpose of preservation, including for adding to the digital archives of the University of Tartu until the expiry of the term of copyright, my thesis

Assessment of lipid nanoparticle-mediated Cre mRNA delivery in cancer cell lines,

supervised by Ph.D. Vladimirs Piļipenko, Prof. Tambet Teesalu, Prof. Juhan Sedman;

2. grant the University of Tartu a permit to make the thesis specified in point 1 available to the public via the web environment of the University of Tartu, including via the digital archives, under the Creative Commons licence CC BY NC ND 4.0, which allows, by giving appropriate credit to the author, to reproduce, distribute the work and communicate it to the public, and prohibits the creation of derivative works and any commercial use of the work until the expiry of the term of copyright;

3. am aware of the fact that the author retains the rights specified in points 1 and 2;

4. confirm that granting the non-exclusive licence does not infringe other persons' intellectual property rights or rights arising from the personal data protection legislation.

Berit Hiie

19/05/2026